

promoting access to White Rose research papers



Universities of Leeds, Sheffield and York
<http://eprints.whiterose.ac.uk/>

This is an author produced version of a paper published in **Wear**.

White Rose Research Online URL for this paper:
<http://eprints.whiterose.ac.uk/4954/>

Published paper

Fouvry, S., Wendler, B., Liskiewicz, T., Dudek, M. and Kolodziejczyk, L. (2004)
Fretting wear analysis of TiC/VC carbides multilayers: Experiments and modelling approaches. *Wear*, 257 (7-8). pp. 641-653.

<http://dx.doi.org/10.1016/j.wear.2004.02.009>

Wear analysis of TiC-VC carbides multilayers: Experiments and modelling approaches

S. FOUVRY^{a*}, B. WENDLER^b, T. LISKIEWICZ^{a,b}, M. DUDEK^{b,a}, L. KOLODZIEJCZYK^{b,a}

^a Laboratoire de Tribologie et de Dynamique des Systèmes, UMR CNRS 5513, Ecole Centrale de Lyon, 36 Avenue Guy de Collongue BP163, 69131 Ecully, France

^b Institute of Materials Science and Technology, Technical University of Lodz, ul. Stefanowskiego 1, 90 924 Lodz, Poland

* *Corresponding author: siegfried.fouvry@ec-lyon.fr*

Abstract : TiC-VC multilayered hard coating were obtained using an original two step hard coating process. Xray analysis, micro-hardness measurements and GDMS's chemical profiles have been conducted to characterise, respectively, crystallography, hardness and multilayer structure as a function of the sub-layer thickness. It shows that although well TiC and VC carbide textures are maintained, a decrease of the sublayer thickness promotes inter-diffusion phenomena which progressively erase the alternated structure. The micro-hardness variation as a function of sublayer thickness displays a parabolic evolution with maximum hardness for a critical thickness around 50 nm. Consistent with the dislocation moving force theories, these results confirm that the micro-hardness evolution is function of the carbide grain size. Wear and friction properties have been studied under gross slip fretting conditions. A “composite” wear model, which considers the diffusion inter-layer, has been developed. Unlike classical rules of mixtures, the modulation dependence of wear and friction is here considered. Reliable wear rates as a function the modulation thickness can be predicted. The friction evolution is less easily predicted due to the smoothing effect of third body. Finally, the opposite evolution between wear resistance and micro-hardness is discussed, outlining the necessity of avoiding any direct prediction of a given tribological response from a plain micro-hardness measurement.

Keywords : Multilayer coating, Tribology, Wear, Fretting, Friction

1. INTRODUCTION

Wear induced by fretting commonly refers to material removal due to repeated sliding of two contacting surfaces over small relative displacements, with amplitudes typically in the 10-100 μm range. Examples of practical situations where fretting wear and fretting cracking influence mechanical integrity include such diverse applications as key-way-shaft and shrink-fitted coupling or biomechanical applications like hip joint prosthesis contact. To limit wear, numerous coatings have been developed and studied [1]. Although single layer coatings suit a wide range of applications in many sectors of engineering, there is an increasing number of sectors where the properties of a single material are not sufficient. Thus, there is need to find coatings that are better suited to such applications. One way to overcome this problem is to use a multilayer coating that combines the attractive properties of several materials [2]. The technologically and economically significant aims of these coatings are the improvement of wear resistance, reduction of the friction coefficient and corrosion protection [3, 4]. Furthermore, coatings can also fulfil other functional tasks (i.e. biocompatibility, thermal barrier) as well as ecological and decorative functions. The present study focuses on the structure and friction properties of modulated TiC-VC multilayered hard coatings. The multilayer hard coating is characterised through micro-hardness measurements and physico-chemical analysis. Wear and friction behaviours under gross slip fretting situations are successively investigated. A composite wear model is developed to predict the kinetic of multilayer hard coatings based on the wear properties of the corresponding monolayer hard and taking into consideration the mixed carbide structure generated by mutual interdiffusion between sublayers. The applications and limits of the approach are discussed in relation to the thickness of the sublayers.

2. TiC-VC MULTILAYERS

2.1 Coating Process

Pure metallic layers are deposited onto a M2 High speed steel substrate by PVD magnetron sputtering (Figure 1) [5, 6]. A small negative bias voltage (-50V) is applied to the components during deposition. This results in ion polishing of the coating surface which promotes dense structure without significant resputtering. After the deposition process, samples were annealed at 1150°C for 1 hour in a vacuum furnace (with residual pressure of 10^{-3} to 10^{-4} Pa). During annealing carbon diffuses from the steel activated by the high temperature and generates TiC

and VC carbides. After the annealing process, the samples were oil quenched and twice tempered at 550°C for 1 hour in order to decrease the internal stress that arose during quenching. An important concept in the production of multilayer coatings is the multilayer period “ λ ” (i.e modulation parameter or superlattice parameter), which is the spacing of the repetition in the structure. To evaluate the influence of the multilayer structure, coatings with the following “ λ ” modulation parameters have been realised ($\lambda = 4.0 \mu\text{m}, 2 \mu\text{m}, 0.8 \mu\text{m}, 0.2\mu\text{m}, 67\text{nm}, 15 \text{ nm}, 4 \text{ nm}$). The number of double layers was adjusted to obtain a constant total thickness around $4 \mu\text{m}$ (respectively $n\lambda = 1, 2, 5, 20, 60, 265, 1000$; $n\lambda$: number of bilayers). Considering the growth rates of Ti and V, which are respectively, 95 nm/min and 44 nm/ min, the exposure time was adjusted to obtain similar sublayer thicknesses (i.e. $\lambda = e_V + e_{Ti}$ and $e_V = e_{Ti}$). Note that both TiC and VC display a cubic structure inducing isostructural multilayers.

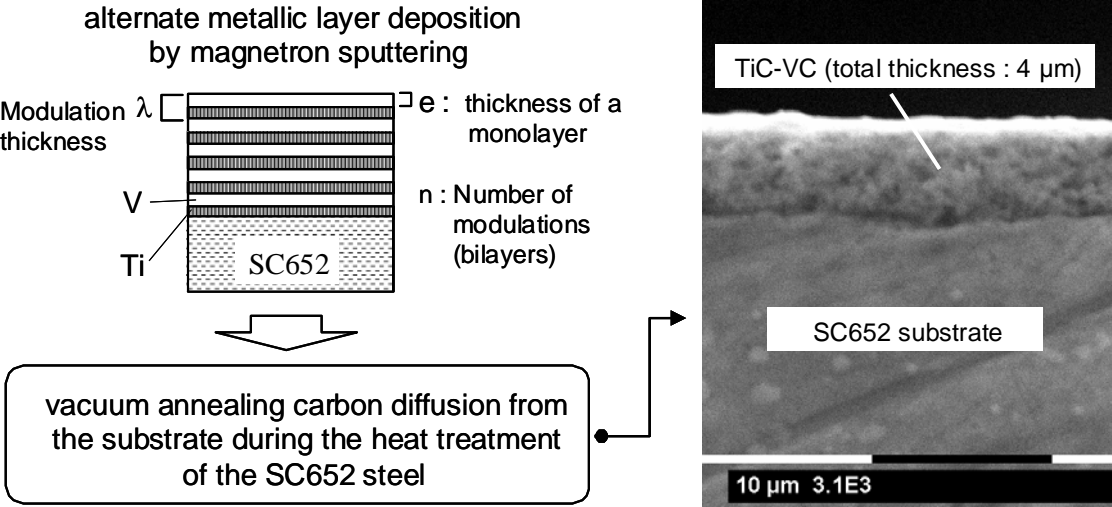


Figure 1 : Illustration of the two step hard coating process.

2.2 Carbide structures

Figure 2 confirms that after vacuum annealing, the metallic sublayers (Ti,V) have been transformed into the corresponding carbide ones (TiC, VC).

The combinaison of the two X-ray patterns indicates that even for the low modulation value ($\lambda=4 \text{ nm}$) well-defined TiC and WC carbide structures are identified. However, the larger scattering observed for the thinner modulation indicates that some diffusion phenomena have been activated leading to alloyed carbides (Ti, V) C. Based on this investigation it can be

concluded that rather well defined carbides have been obtained although no clear information is available concerning the layered structure of the coating after the annealing treatment.

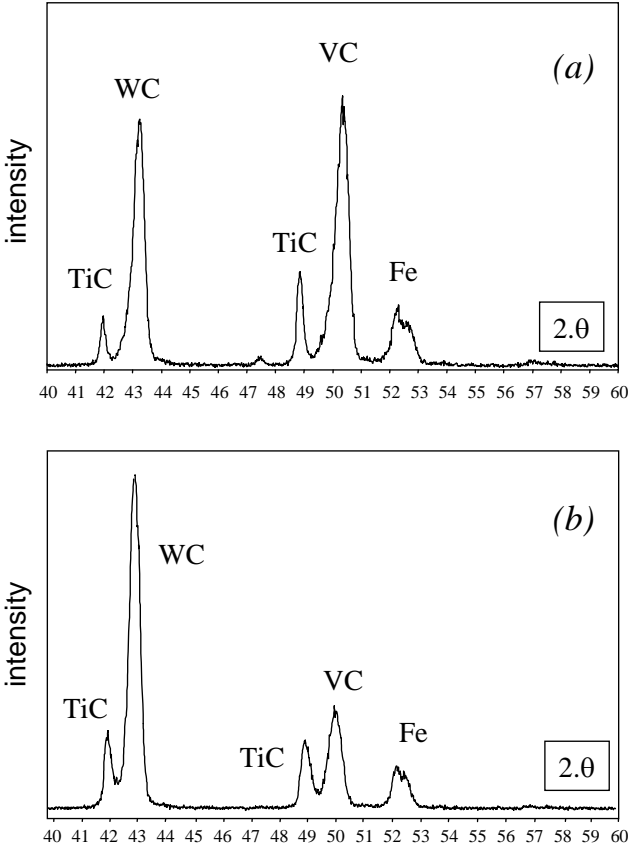


Figure 2 : X-ray patterns of multilayer Ti/V after vacuum annealing: (a) $\lambda = 4.0 \mu\text{m}$; (b) $\lambda = 4 \text{ nm}$ (Co $K\alpha$ radiation and graphite monochromator).

2.3 Layered structure

In order to identify the layered structure of the studied carbide coatings, GDMS (Glow Discharge Mass Spectroscopy) profiles have been conducted before and after the annealing treatment (Figure 3). This semi quantitative chemical analysis, based on continuous ion sputtering, allows us to measure the relative concentration of chemical elements like C, V, Ti and Fe through the coating and near the substrate interface. Compared to SIMS spectroscopy, it displays worse spatial resolution (few mm^2). But the speed of this technique (a few seconds) allows for thicker coating analyses (up to $6 \mu\text{m}$). However, the deeper the analysis, the greater the risk of analysing several layers, leading to the dispersion of the chemical profiles. This limitation is clearly illustrated in Figure 3c where well-defined square patterns are observed in the first $2 \mu\text{m}$ depth compared to the less defined inner profiles. Another limitation of this

technique is the non-direct correlation between sputtering time and the absolute position through the coating.

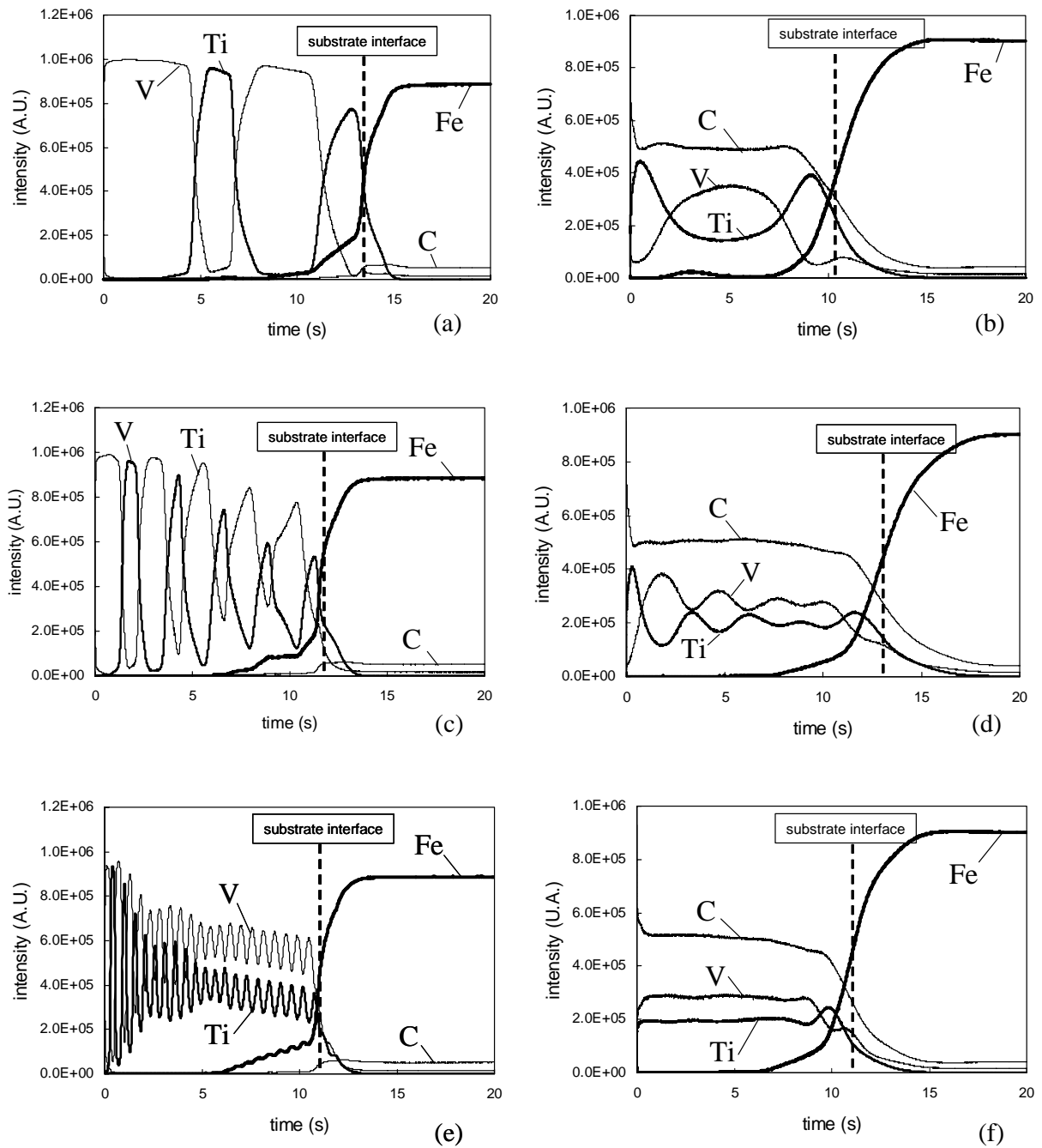


Figure 3 : GDMS Chemical profiles of the multilayers as a function of sputtering time; One bilayer system ($\lambda = 4.0 \mu\text{m}$): (a) metallic layer, (b) after annealing; five bilayer system ($\lambda = 0.8 \mu\text{m}$): (c) metallic layer, (d) after annealing; twenty bilayer system ($\lambda = 0.2 \mu\text{m}$): (e) metallic layer, (f) after annealing.

The presence of iron through the inner part of the coating suggests that mutual diffusion has been activated at the substrate interface promoting good adhesion properties.

By comparing the metallic and carbide layers, it can be seen that mixing phenomena have been activated near the sublayer interfaces during the annealing process. Interdiffusion between V and Ti is observed and tends to be predominant, decreasing the modulation parameter. A completely mixed TiC-VC layer seems to be observed for modulation values lower than 0.2 μm (i.e. $n\lambda > 20$). This limit must be considered with caution because of the wide scattering of the technique. It only confirms that for modulation values higher than 0.2 μm a TiC-VC layered structure is maintained, and suggests that a fully mixed carbide structure is obtained for modulation thicknesses between 0.2 μm and 67 nm, which corresponds to a critical number of sublayers around 40.

2.4 Hardness properties

Figure 3 shows the evolution of the micro hardness versus the modulation parameter. It can be compared to the corresponding values obtained on single TiC and VC respectively 2500 and 3000 Hv.

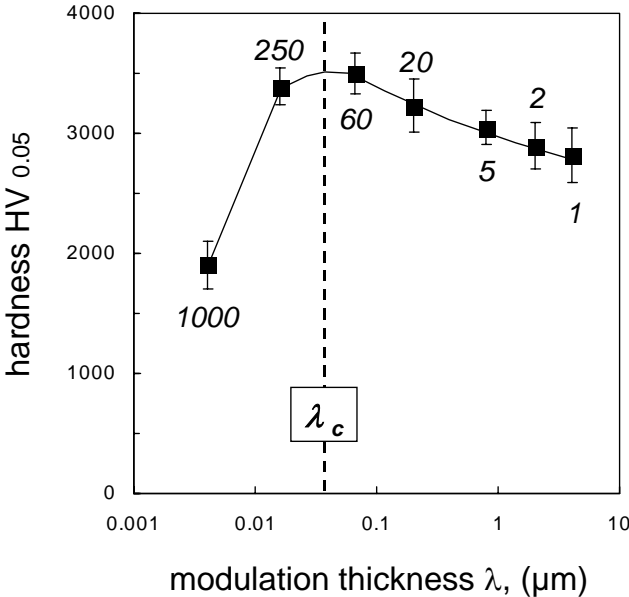


Figure 2 : Effect of the modulation parameter λ on the microhardness of TiC-VC multilayers (60 : $n\lambda$ number of modulations).

Decreasing the modulation parameter tends to increase the hardness [7], which becomes higher than that of the vanadium carbide for a modulation value lower than 2 μm . This monotonic

evolution is nevertheless observed until a critical value around $\lambda_c = 50$ nm that corresponds to maximum micro hardness. Below this modulation value, the micro hardness tends to decrease down to very low hardness around 2000 Hv. Note that the maximum hardness condition ($\lambda_c \approx 50$) does not exactly correspond to the pure mixed carbide structure ($\lambda \approx 100$). This shows that no direct correlation can be drawn between the micro-hardness properties and the sublayer inter-diffusion phenomena. Such a tendency was previously confirmed on TiN/NbN superlattices by Yashar and Sproul [7] and by other authors [8, 9] for different carbide and nitride PVD deposited superlattice coatings. Anderson and co-authors also observed a similar micro-hardness evolution for metallic structure like Cu/Ni multilayers [10]. They developed a complete model based on the calculation of the critical shear stress required for the dislocation loop moving within a given layer, and the determination of the dislocation density in the cell. The model takes into account the effects of a mismatch between the layers, the image forces on dislocations related to the elastic differences between sublayers, the dislocation core spreading into the interface, the structural differences between the layers, the difference in stacking fault energies, and the creation of a residual dislocation left at the interface after a dislocation passes. One major interest of this approach is that it predicts the overall behaviour of the micro-hardness evolution as a function of the modulation thickness. At large modulation (i.e. $\lambda > 100$ nm), dislocation motion is impeded at the interfaces and corresponds to the classical Hall-Pech description where the microhardness appears to be proportional to $\lambda^{-1/2}$. However, the curve levels off and reaches a maximum at $\lambda \approx 10$ nm. This corresponds to the situation where there is only space in the sublayer for one dislocation. As the modulation is reduced, the thickness at which misfit dislocations between sublayers no longer appears, the dislocation can more easily pass through the interfaces and a large drop in yield strength and consequently hardness is observed. However, this multilayer description displays two inconsistencies with the present experiments. First, the critical length defined by the model (10 nm) is significantly lower than the critical modulation presently defined (50 nm). Secondly, GDMS analyses confirm that for λ smaller than 70 nm the alternate layered structure is completely erased after the heat treatment.

These two inconsistencies can partly be resolved if, rather than considering the λ modulation thickness, the analysis focuses on carbide grain size generated during the heat treatment. A proportional reduction of the grain size with the modulation value can be assumed and more than one grain could be generated through the sublayer thickness. That could explain the difference in terms of critical length (λ_c). Moreover, if well established carbides are

generated, as confirmed by the X-ray patterns, below a critical modulation thickness, the alternated VC and TiC multilayer structure no longer exist. The Anderson and co-authors model is again applicable if rather than considering the layered approach, the analysis is transposed to an adjacent tridimensional subgrain structure.

3. TRIBOLOGICAL PROPERTIES OF TiC-VC MULTILAYERS

3.1 Test conditions

Fretting tests were carried out using an electrodynamical shaker activating a specific fretting ring illustrated in Figure 5. A 12.7 mm radius polycrystalline alumina ball was used as a counterbody [11]. Tests were conducted in a closed chamber where the ambient humidity is controlled (50%). A 100 N normal load up to a maximum pressure around 1400 MPa was imposed. A constant $\pm 100\mu\text{m}$ displacement amplitude was applied with a 5Hz frequency and a number of fretting cycles from 5000 to 25000. Both the tangential force (Q) and displacement (δ) are recorded; thus the fretting loop ($Q=f(\delta)$) can be plotted to extract quantitative variables including the sliding amplitude (δ_g), the displacement amplitude (δ^*) and the tangential force amplitude (Q^*). The wear volume, contact radius and maximum wear depth were measured using 3D surface profilometries.

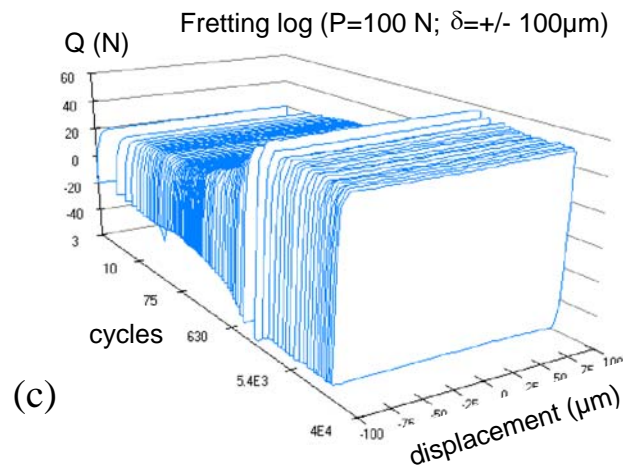
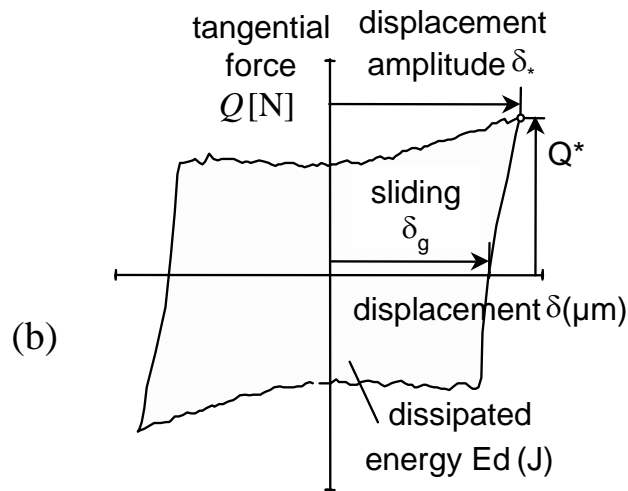
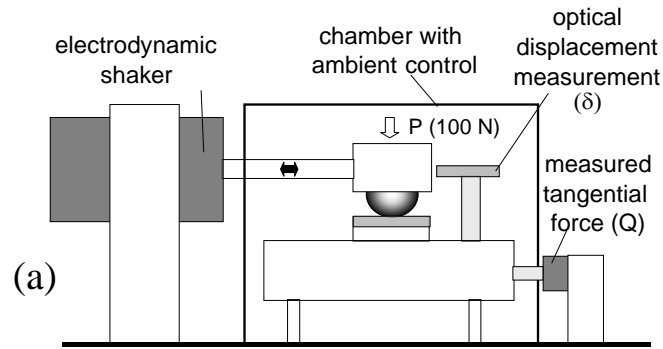


Figure 5 : Illustration of the experimental fretting wear approach : (a) schematic of the fretting rig, (b) analysis of the fretting cycle, (c) Fretting log (i.e. the fretting cycles are reported along a logarithmic time scale).

3.2 Methodology to quantify wear

The classical wear coefficient (K) defined from Archard's description is considered [11].

Wear volume extension is compared to the product of the normal force (P) and the accumulated sliding distance (S). For fretting sliding, the Archard expression is derived as

follow:

$$K = \frac{V}{W} = \frac{V}{\sum_{i=1}^N 4 \cdot \delta_{gi} \cdot P_i} \quad \text{with } W = P \cdot S \quad (1)$$

3.3 Friction and Wear behaviour of monolayer system

The major aim of this study is to define how the wear kinetics of a multilayer could be extrapolated from monolayer systems. This implies prior characterisation of monolayers TiC, VC coating responses. Both TiC and VC monolayer coatings have been made using a similar two-step annealing process. Figure 6 illustrates the friction behaviour of the two coatings, which confirms the lower friction value of TiC under fretting.

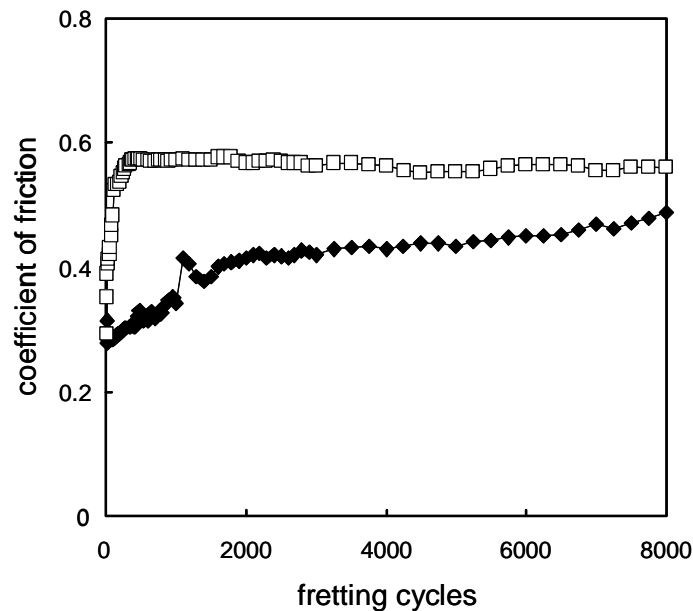


Figure 6 : Coefficient of friction versus fretting cycles ($P=100\text{ N}$, $\delta^*=\pm 100\mu\text{m}$); \square , VC against alumina; \blacklozenge , TiC against alumina.

The averaged analysis of the whole tests gives mean values of 0.45 and 0.63 respectively for the studied TiC and VC structures.

Figure 7 confirms the higher wear resistance of the VC structure compared to the TiC carbide.

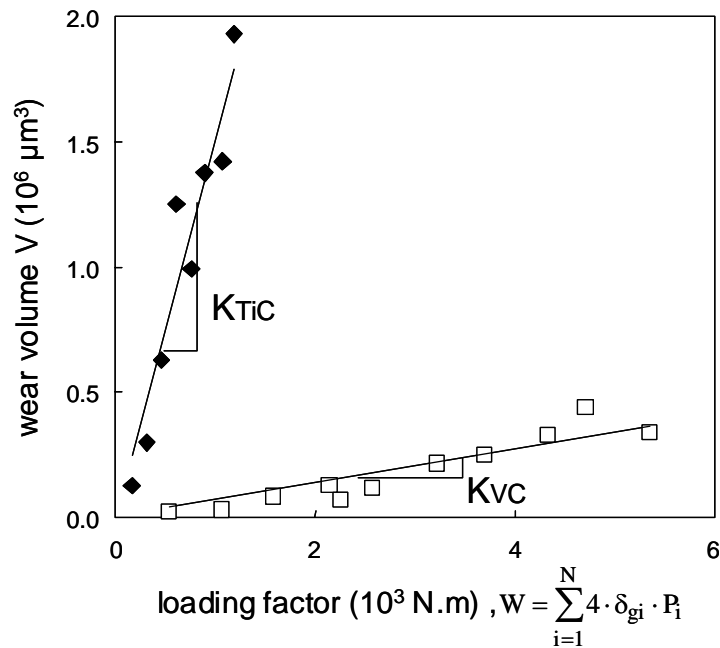


Figure 7 : Evolution of the wear volume versus the product of the normal force and the sliding distance (W factor) : ($P=100 \text{ N}$, $\delta^*=+/-100\mu\text{m}$, fretting cycles : 5000-200000); □, VC / alumina; ◆, TiC / alumina.

The different tribological data extracted from this fretting study are reported in Table 1.

Table 1 : Tribological properties of the studied TiC and VC monolayers under fretting loadings.

	mean coefficient of friction : $\bar{\mu}$	K ($\mu\text{m}^3/\text{N.m}$)
TiC/alumina	0.45	1500
VC/alumina	0.63	70

3.4 Tribological properties of modulated multilayers.

3.4.1 Friction Behaviour

Figure 8 shows the friction evolution of a $(\text{TiC}/\text{VC})_2$ bi-modulation coating. The transition from VC to the TiC sublayers is clearly marked by discontinuities of the coefficient of

friction. Such a friction transition can be related to the wear depth extension through the coating and the passage between carbide sublayers.

The fluctuation nevertheless smooths out: after a given wear extension several carbide layers are involved through the interface, and the third body that controls the friction behaviour includes a mixture of the different carbides.

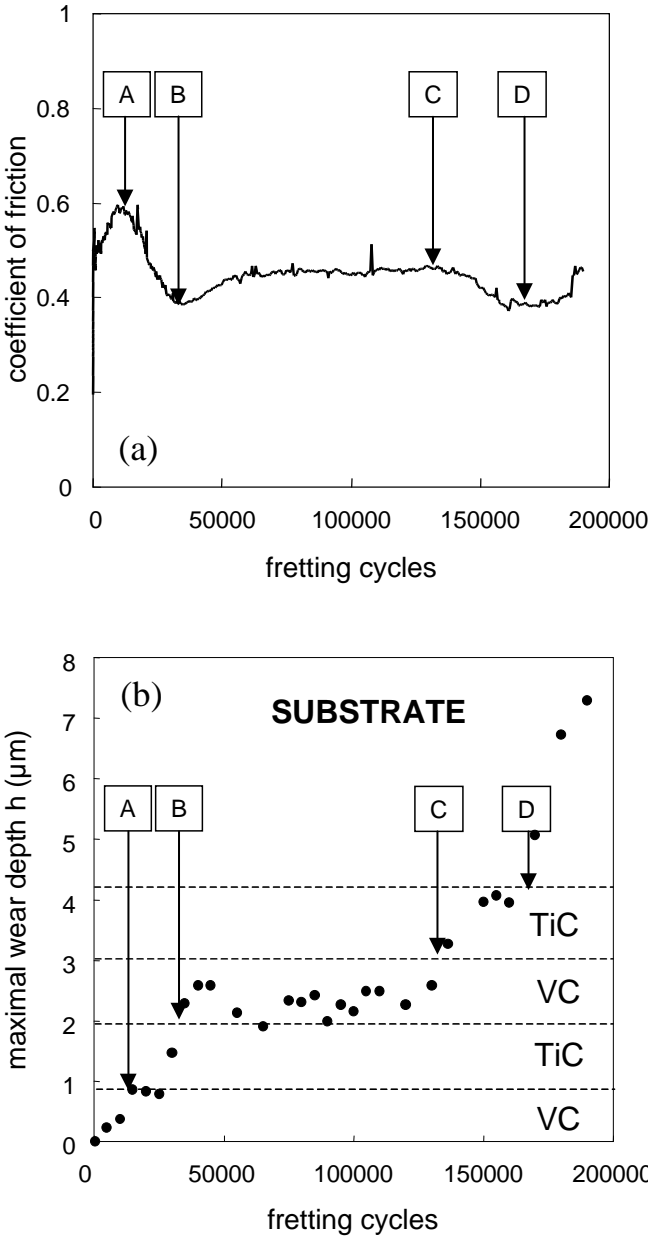


Figure 8 : Correlation between the coefficient of friction (a) and the wear depth extension through the carbide sublayers (b) : two bilayer system (TiC-VC)₂ ($\lambda \approx 2 \mu\text{m}$).

The interface tends then to a composite carbide structure displaying a quasi periodic annular structure (Figure 9) where the major part of the exposed interface concerns the deeper layer.

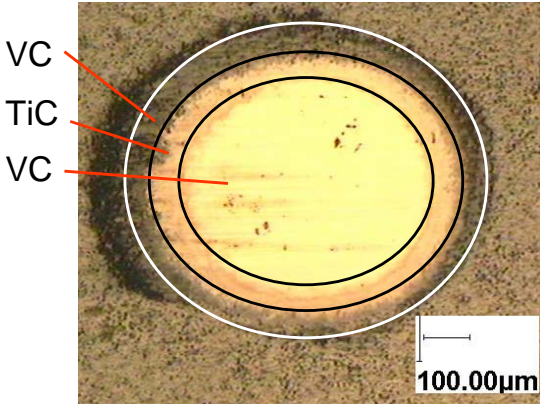


Figure 9 : Surface observation of the two bilayer system (TiC-VC)₂ after 100000 cycles.

To characterise the multilayer friction behaviour, a mean friction value is determined until the substrate is reached. Figure 10 compares the evolution of the mean friction value as a function of the modulation parameter (λ). The friction values are constrained between the two single layer coatings. A smooth increase of the friction values with the modulation thickness is nevertheless observed.

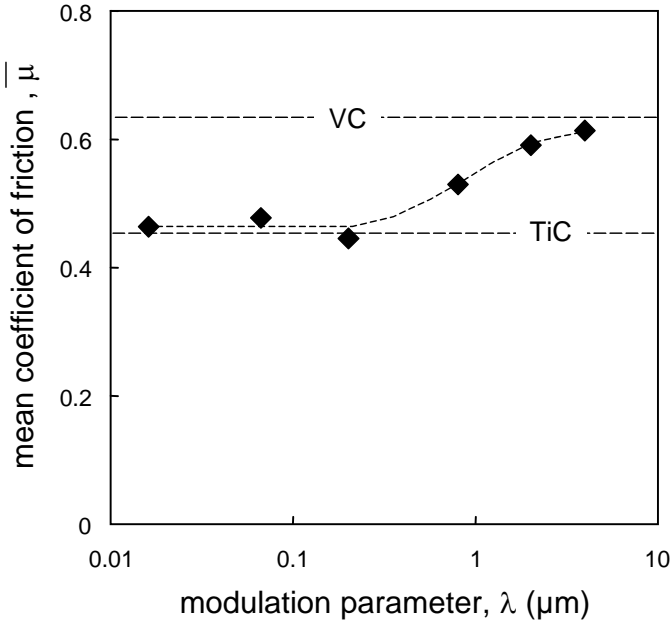


Figure 10 : Evolution of the coefficient of friction as a function of the modulation parameter.

3.4.1 Wear volume analysis

Figure 11 illustrates the wear volume extension for the different multilayer structures.

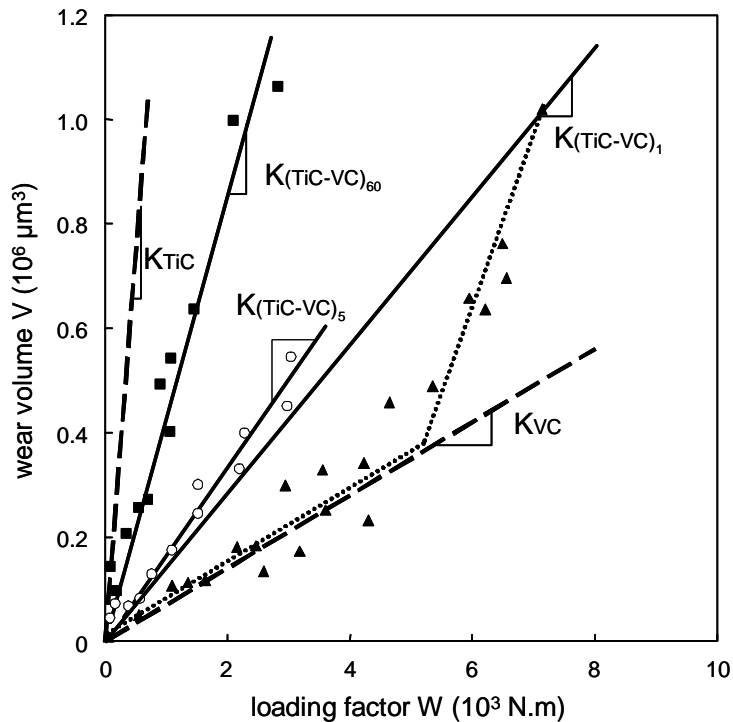


Figure 11 : Evolution of the wear volume versus the product of the normal force and the sliding distance (W factor) : Comparison between monolayer (Figure 7) and multilayer behaviours ($P=100$ N, $\delta^*=+/-100\mu\text{m}$, fretting cycles : 5000-200000); ■ $(\text{TiC-VC})_{60}/\text{alumina}$; ○ $(\text{TiC-VC})_5/\text{alumina}$; ▲ $(\text{TiC-VC})_1/\text{alumina}$.

The comparison indicates that all the multilayer wear kinetics are between the TiC and VC wear rates. It also shows that the wear kinetics tend to increase as the modulation parameter decreases. However some differences are observed. For the one bilayer system, as long as the first layer in contact is VC, the wear kinetics are the same as for the monolayer VC carbide. Passing through the interface, wear sharply increases and tends to the TiC wear kinetics. Hence a wear discontinuity is identified that marks the transition between two wear regimes. It outlines the difficulty in identifying the averaged wear coefficient which, for such a case, implies considering the ultimate moment when the substrate is reached. When the sublayer thicknesses decreases, the discontinuities are smooth out and the averaged wear coefficient can directly be derived from a linear approximation.

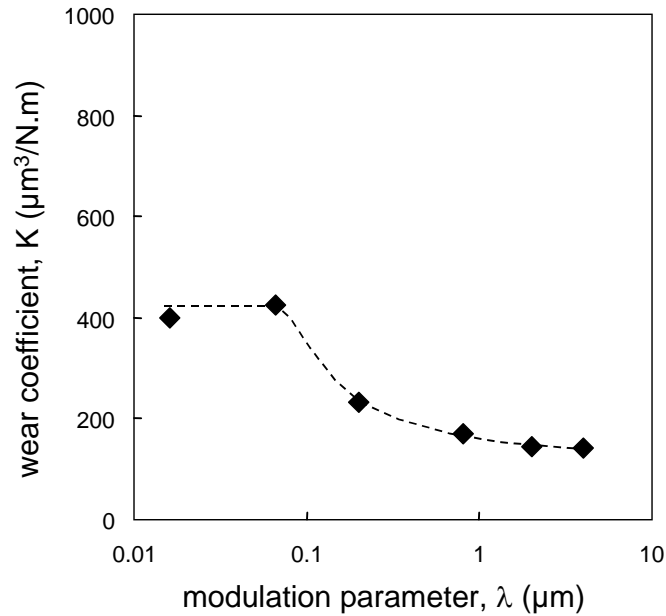


Figure 12: Evolution of the wear coefficients as a function of the modulation parameter,

Figure 12 plots the evolution of the wear coefficient as a function of the modulation thickness. It confirms the increase of the wear coefficient up to a stabilised value (around $400 \mu\text{m}^3/\text{N.m}$) as the modulation decreases.

The different tribological properties (friction, wear coefficients) defined for the studied multilayers are reported in Table 2.

Table 2 : Tribological properties (friction and wear coefficients) of the studied TiC-VC modulated multilayers.

Modulation parameter : λ (μm)	4	2	0.8	0.2	0.066	0.016
(number of modulations: $n\lambda$)	(1)	(2)	(5)	(20)	(60)	(250)
Mean coefficient of Friction : $\bar{\mu}$	0.61	0.59	0.53	0.45	0.48	0.46
Wear coefficient K ($\mu\text{m}^3/\text{N.m}$)	143	145	170	233	425	400

3.5 Modelling of the tribological properties.

3.5.1 Topography of the wear scars

Unlike grinder tests, which are widely employed to analyse the abrasion resistance of multilayers, the topography of the fretting scars presents a rather flattened square profile (Figure 13).

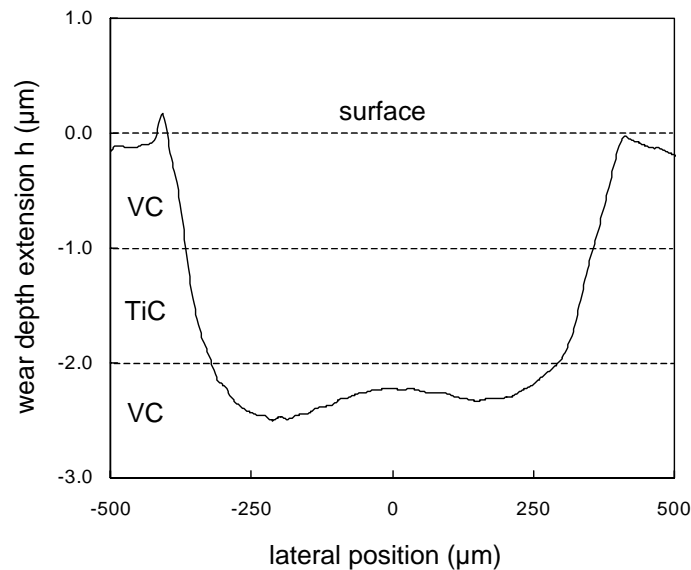


Figure 13 : Cross profile of the *two bilayer system (TiC-VC)₂* after 100000 cycles (Fig. 9).

Indeed, classical grinder tests impose a continuous change of the counterbody interface, and the spherical shape is consequently maintained [13]. Under fretting or reciprocating conditions, the fretted surfaces are always the same. The shape of the counterbody interface is rapidly modified, passing from a spherical to a flattened surface morphology as illustrated in Figure 14. The surface wear induces an increase of the contact area and a proportional decrease of the pressure field. This latter evolves from a classical Hertzian elliptical distribution with a maximum at the center toward a rather homogeneous mean pressure field distribution. It infers a homogeneous wear depth extension characterising the flattened wear profiles measured on the coating fretting scars. Considering such a morphology, different wear models have been developed and compared.

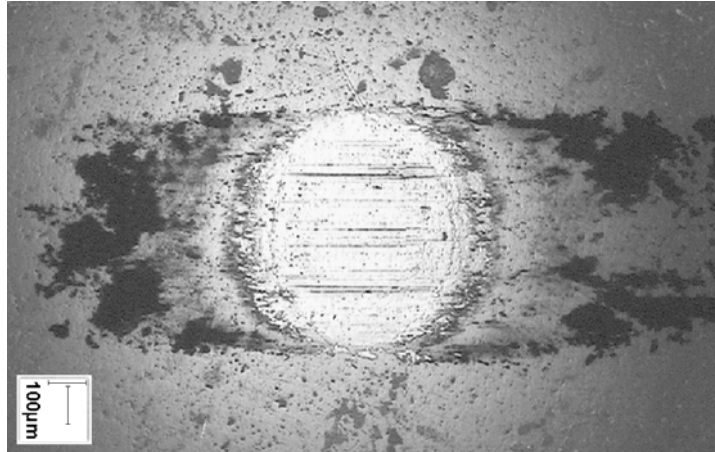


Figure 14 : Optical observation of the alumina interface after 10000 cycles.

3.5.2 Perfectly layered structure

This first description considers a perfectly layered structure without any diffusion between sublayer interfaces (Figure 15). Each layer “ i ” is then characterised by its thickness “ $e(i)$ ” its wear coefficient “ $K(i)$ ” and the corresponding friction value “ $\bar{\mu}(i)$ ”. Each constituent property can be defined from the corresponding monolayer coating tribological analysis. The modulation element is then defined by superposing of the different constituent sublayers.

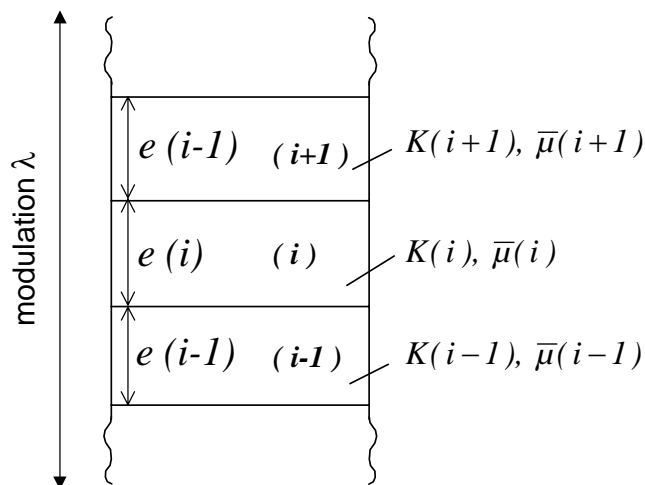


Figure 15 : Illustration of the multilayer considering a perfectly layered structure.

Layered wear model

Assuming homogeneous pressure field distribution and homogeneous wear depth extension, the wear volume analysis can directly be extrapolated from a simple surface integration over

the whole fretting scar (Figure 16). If a unit element surface is considered, the wear depth extension (h) is then compared to the accumulated local product of the sliding and the mean pressure (W_h).

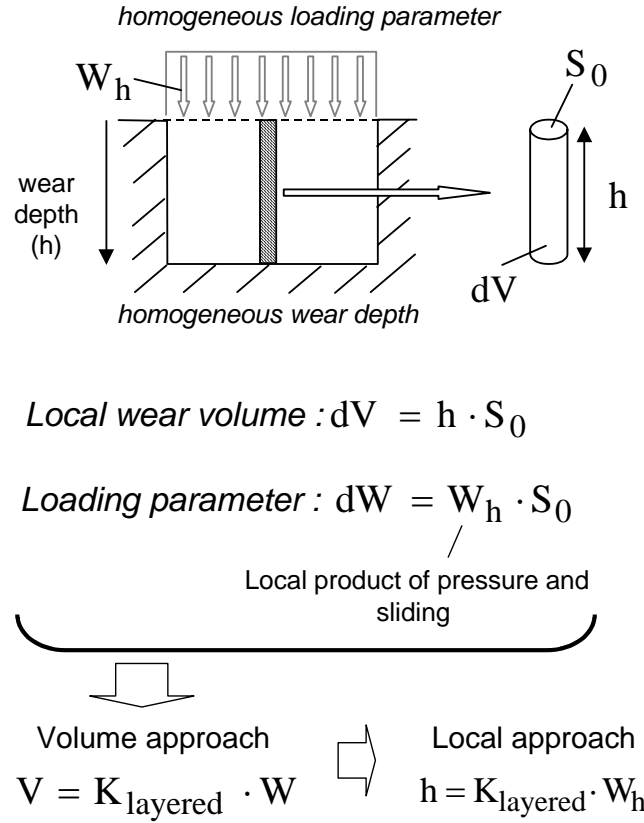


Figure 16 : Illustration of the local wear analysis, S_0 unit surface element.

Transposed to the multilayer wear depth analysis, a layered wear energy coefficient is identified:

$$K_{\text{layered}} = \frac{\lambda}{\sum_{i=1}^N e_i / K_i} \quad (2)$$

which presently, for the bilayer system, leads to the simplified expression (Figure 17).

$$K_{\text{layered}}[\text{TiC} - \text{VC}] = \frac{\lambda}{e_{\text{TiC}}/K_{\text{TiC}} + e_{\text{VC}}/K_{\text{VC}}} = \frac{2}{1/K_{\text{TiC}} + 1/K_{\text{VC}}} \quad (3)$$

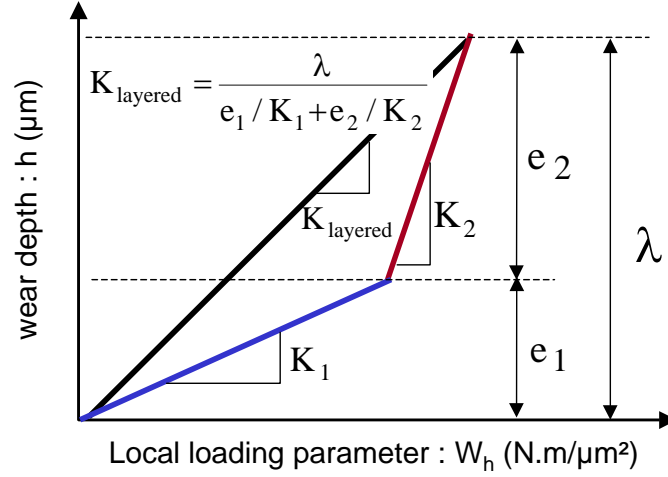


Figure 17 : Illustration of the layered wear approach based on an incremental wear depth description (application to the bi-layer system).

As predicted by the model, fluctuations of the wear extension could be observed, which depended on the passage from one to successive sublayers. This confirms the discontinuities observed for thickest modulations (Figure 8b and Figure 11) and implies that the substrate reaching condition must be considered in order to correctly define a representative averaged wear rate. For the studied structure, a constant value ($K_{\text{layered}}[\text{TiC-VC}] \approx 133 \mu\text{m}^3 / \text{N.m}$) has been determined. Like any rules of mixtures wear rate formulations, the calculated wear rate is between the two constituent phases [14].

Layered friction model

A “layered” friction value is also defined how long each carbide layer is in contact with the counterbody. In addition to the sublayer thickness, this analysis integrates the corresponding wear coefficients. A general expression is derived and expressed as followed :

$$\bar{\mu}_{\text{layered}} = \frac{\sum_{i=1}^N \left(\frac{e_i}{K_i} \cdot \bar{\mu}_i \right)}{\sum_{i=1}^N \frac{e_i}{K_i}} \quad (4)$$

With ‘N’ the number of sublayers through the modulation element.

It can be simplified for the bilayer system through this relationship:

$$\bar{\mu}_{\text{layered}}[\text{TiC-VC}] = \frac{1}{e_{\text{TiC}} / K_{\text{TiC}} + e_{\text{VC}} / K_{\text{VC}}} \cdot \left(\frac{e_{\text{TiC}}}{K_{\text{TiC}}} \cdot \bar{\mu}_{\text{TiC}} + \frac{e_{\text{VC}}}{K_{\text{VC}}} \cdot \bar{\mu}_{\text{VC}} \right) \quad (5)$$

The layered friction value estimated for this multilayer system is around 0.62. This value is very close to the VC coefficient of friction which can be explained by the higher wear resistance of VC that corresponds to longer contact time between this constituent and the alumina counterbody (Figure 8b).

3.5.3 The mixed layer approach

Friction and wear analyses show the limitation of the perfectly layered models, which can not clarify the impact of modulation thickness on tribological properties. To interpret these limitations, the mixed carbide layer resulting from interdiffusion phenomena between the sublayers must be taken into consideration. Inspired from the Berger and Co-workers analysis [13], the previous layered structure is deepened considering a mixed layer (e_m) which is assumed to display a constant thickness independent of the modulation value (Figure 18).

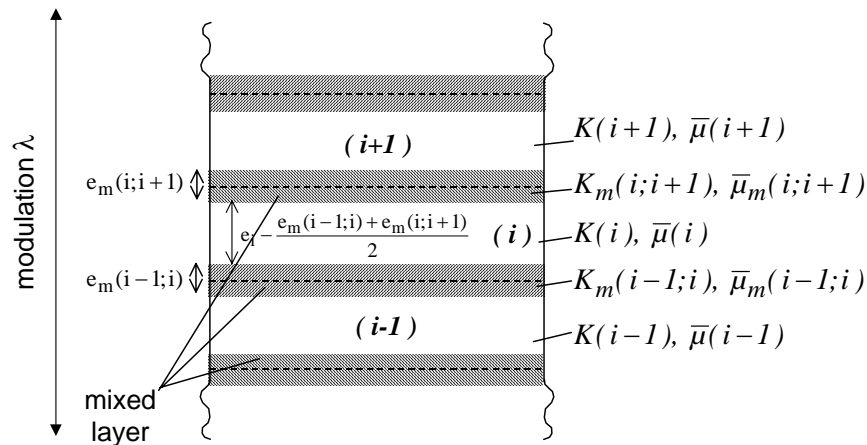


Figure 18 : Illustration of the multilayer structure taking into account the interdiffusion mixed layers between the constituent sublayers.

If the mixed layer is assumed to extend equally toward the adjacent sublayers, decreasing the modulation thickness will induce a proportional decrease of the well-defined sublayers (Figure 17) until to a pure mixed structure ($\lambda = N \cdot e_m$) is obtained.

Composite wear model

For thicker modulation thicknesses, the layered approach still operates. A composite wear coefficient is then expressed.

$$K_{\text{composite}} = \frac{\lambda}{\sum_{i=1}^N \left(\frac{1}{K(i)} \cdot \left(e^{(i)} - \frac{e_m(i-1;i) + e_m(i;i+1)}{2} \right) \right) + \sum_{i=1}^N \left(\frac{e_m(i-1;i)}{2 \cdot K_m(i-1;i)} \right) + \sum_{i=1}^N \left(\frac{e_m(i;i+1)}{2 \cdot K_m(i;i+1)} \right)} \quad (6)$$

with:

$e_m(i-1;i)$: Constant thickness of the lower mixed layer between sublayers $i-1$ and i ,

$e_m(i;i+1)$: Constant thickness of the upper mixed layer between sublayers i and $i+1$,

$K_m(i-1;i)$: Wear coefficient of the inferior lower layer defined from interdiffusion between sublayer $i-1$ and i .

$K_m(i;i+1)$: Wear coefficient of the upper mixed layer defined from interdiffusion between sublayer i and $i+1$.

For the simple studied bi-carbide structure ($N=2$) the latter expression leads to the simplified expression:

$$K_{\text{composite}}[\text{TiC} - \text{VC}] = \frac{\lambda}{(e_{\text{TiC}} - e_m)/K_{\text{TiC}} + (e_{\text{VC}} - e_m)/K_{\text{VC}} + 2 \cdot e_m / K_m} \quad (7)$$

The application of such a layered wear model, requires to both the mixed layer thickness and the corresponding wear coefficient, to be identified.

This can be achieved by considering the limit condition when all coating tends to a global mixed structure. This condition is reached when $n\lambda=40$, which implies a mixed layer thickness around $e_m \approx 0.05 \mu\text{m}$ and $K_m \approx 400 \mu\text{m}^3 \cdot (\text{N} \cdot \text{m})^{-1}$. Below this thickness the wear response of the coating is equivalent to that of the mixed carbide structure.

Composite friction model

This composite description is successively transposed to friction analysis. If the mixed carbide layer is considered, the layered formulation (Eq. 4) leads to the following general expression associated to a mean “composite” friction coefficient.

$$\bar{\mu}_{\text{composite}} = \frac{\sum_{i=1}^N \left(\frac{\bar{\mu}(i)}{K(i)} \cdot \left(e^{(i)} - \frac{e_m(i-1;i) + e_m(i;i+1)}{2} \right) \right) + \sum_{i=1}^N \left(\frac{\bar{\mu}_m(i-1;i) \cdot e_m(i-1;i)}{2 \cdot K_m(i-1;i)} \right) + \sum_{i=1}^N \left(\frac{\bar{\mu}_m(i;i+1) \cdot e_m(i;i+1)}{2 \cdot K_m(i;i+1)} \right)}{\sum_{i=1}^N \left(\frac{1}{K(i)} \cdot \left(e^{(i)} - \frac{e_m(i-1;i) + e_m(i;i+1)}{2} \right) \right) + \sum_{i=1}^N \left(\frac{e_m(i-1;i)}{2 \cdot K_m(i-1;i)} \right) + \sum_{i=1}^N \left(\frac{e_m(i;i+1)}{2 \cdot K_m(i;i+1)} \right)} \quad (8)$$

Applied to the bi-layer system, the following simplified formulation is then deduced.

$$\bar{\mu}_{\text{composite}}[\text{TiC} - \text{VC}] = \frac{\bar{\mu}_{\text{TiC}} \cdot \frac{(e_{\text{TiC}} - e_m)}{K_{\text{TiC}}} + \bar{\mu}_{\text{VC}} \cdot \frac{(e_{\text{VC}} - e_m)}{K_{\text{VC}}} + \bar{\mu}_m \cdot \frac{2 \cdot e_m}{K_m}}{\frac{(e_{\text{TiC}} - e_m)}{K_{\text{TiC}}} + \frac{(e_{\text{VC}} - e_m)}{K_{\text{VC}}} + \frac{2 \cdot e_m}{K_m}} \quad (9)$$

Like for wear analysis, the transition towards a pure mixed carbide structure is observed for modulation thicknesses between 67 nm and 0.2 μm . When a similar critical number of sublayers ($n\lambda=40$) is considered, the mixed layer thickness is fixed at $e_m \approx 0.05 \mu\text{m}$ with a corresponding mean friction coefficient around 0.46.

3.5.4 Comparison between experiments and models

Wear analysis

Figure 15 compares the wear models with the experiments. It concludes that as long as well layered structures are present (thickest modulations), the layered model gives a rather fine estimation of the wear kinetics. If the sublayer thickness is decreased, interdiffusion favours the formation of a mixed layer structure at the sublayer interfaces. Therefore when the sublayer thickness becomes too small, the global composition of the coating tends to the mixed layer structure and the “layered formulation”, independent of modulation thickness, is no longer appropriate.

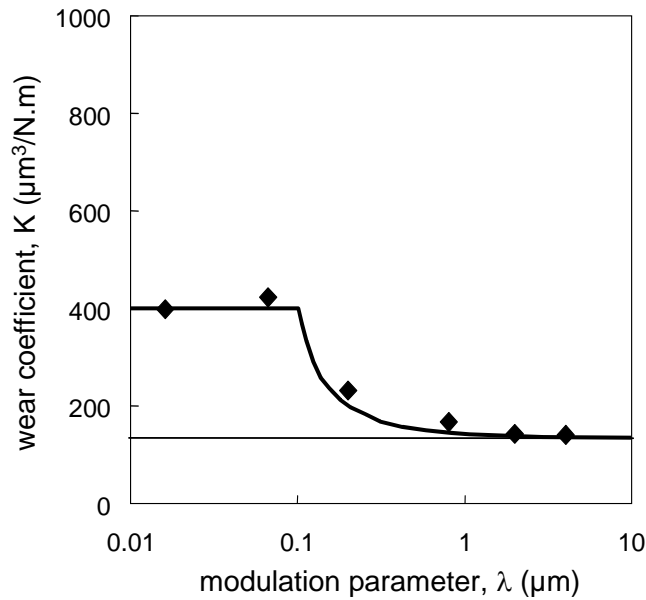


Figure 19 : Wear kinetics of (TiC-VC) multilayers as a function of the modulation thickness; \blacklozenge experimental results (Table 2) ; — Layered wear model (Eq. 3) ; — Composite wear model (Equ. 7); ($K_{\text{TiC}} = 1500 \mu\text{m}^3 \cdot (\text{N.m})^{-1}$, $K_{\text{VC}} = 70 \mu\text{m}^3 \cdot (\text{N.m})^{-1}$, $e_m = 0.05 \mu\text{m}$, $K_m = 400 \mu\text{m}^3 \cdot (\text{N.m})^{-1}$).

Despite its simple rule of mixture form, the composite wear approach agrees very well with the experimental results. Hence the wear kinetics can conveniently be predicted based on a precise description of the constituent carbide sublayers (ie TiC and VC) and taking into account the thickness and wear properties of mixed carbide layers generated by thermal diffusion at the sublayer interfaces. However, the present approach is only transposable to situations displaying homogeneous wear depth extensions. Further developments are now required to extend this description to variable contact morphology and complex pressure field distributions.

Friction analysis

Experimental and models friction evolutions are compared in Figure 20. The layered friction description with a time approach, appears to be a pertinent formalisation as long as well-defined sublayers are maintained (i.e. highest modulation values). Although, when the modulation thickness decreases, it fails again to describe the decrease of the friction behaviour.

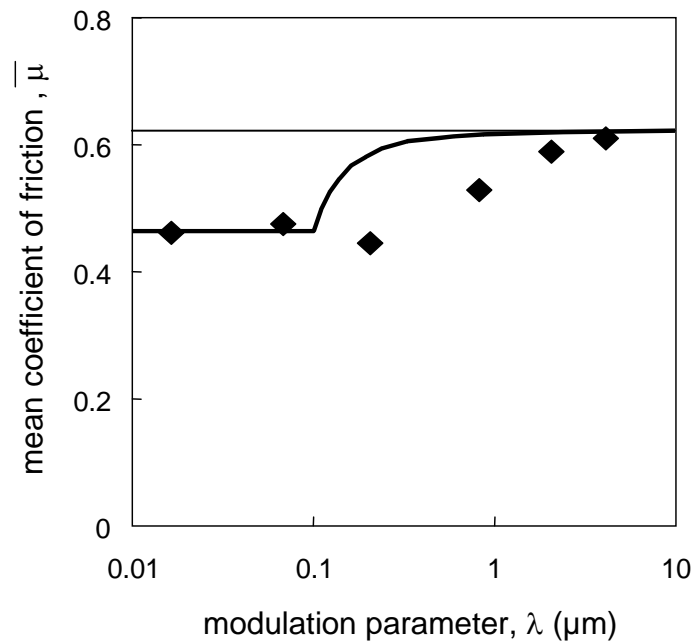


Figure 20 : Friction evolution of (TiC-VC) multilayers as a function of the modulation thickness; \blacklozenge :experiments; — Layered friction model (Eq. 5); — Composite friction model (Equ. 8); ($K_{TiC}= 1500 \mu\text{m}^3 \cdot (\text{N}\cdot\text{m})^{-1}$, $\mu_{TiC} = 0.45$, $K_{VC}= 70 \mu\text{m}^3 \cdot (\text{N}\cdot\text{m})^{-1}$, $\mu_{VC} = 0.6$, $e_m=0.05\mu\text{m}$, $K_m=400 \mu\text{m}^3 \cdot (\text{N}\cdot\text{m})^{-1}$, $\mu_m = 0.46$).

By comparison, the composite friction approach gives a good estimation near the two extreme ranges of modulation thickness (i.e. $\lambda < 0.1 \mu\text{m}$ and $\lambda > 2 \mu\text{m}$). Significant dispersion is nevertheless observed for intermediate values. It appears that the mean friction coefficient tends faster than predicted to the pure mixed carbide structure friction behaviour (0.45). Such dispersion could be related to a third body smoothing effect. Hence, the friction coefficient depends on the composition and structure of the third body. Passing through the successive sublayers, its composition tends rapidly to mixture of carbide and oxides leading to an averaged friction value equivalent to the pure mixed carbide structure. Further developments are here required to better integrate the third body impact on the multilayer friction response by developing a new physical description of the interface.

Finally, using the “composite” approach, the tribological properties can be predicted or at least estimated. This approach can be applied when specific friction and wear resistance properties are required. By adjusting the modulation thickness a compromise could be predicted and defined. Such optimised multilayer prediction is nevertheless restricted to the condition of coherence between the industrial application and the studied fretting situation.

4. CORRELATION BETWEEN STRUCTURAL, HARDNESS AND TRIBOLOGICAL PROPERTIES.

Figure 21 compares the normalised evolution of microhardness, wear resistance (1/K) and friction coefficient as a function of the modulation thickness. Whereas wear resistance and friction present similar tendencies, the opposite evolution is observed between wear resistance and micro-hardness. It clearly outlines the difficulty of linking mechanical and tribological properties [1, 15].

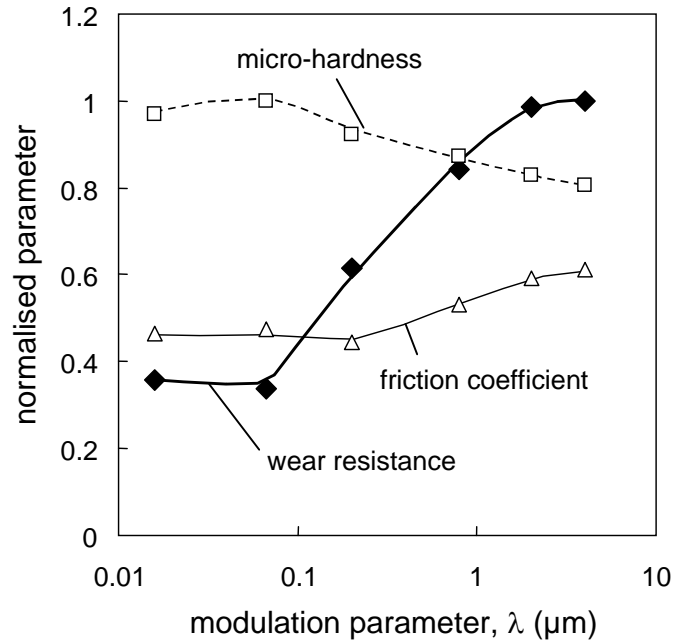


Figure 21 : Normalised comparison between tribological properties (wear and friction) and the micro-hardness of (TiC-VC) multilayers as a function of the modulation thickness (—◆— Normalised wear resistance ($(1/K)/\max(1/K)$); —△— Coefficient of friction; - -□- - Normalised micro-hardness ($H_v/\max(H_v)$)).

It has been shown and explained how micro-hardness evolution of such “two step” multilayer hard coatings is related more to the local carbide subgrain structure and the moving dislocation force rather than to multilayer morphology. Conversely, it has been shown that both wear and friction properties are sharply dependent on the layered structure, and its evolution induced inter-diffusion phenomena. Such a difference in terms of mixed carbide dependence is also verified regarding the quantitative values. Indeed, if tribological properties (wear resistance and coefficient of friction) can be extrapolated by composite “mixture” rules, this is absolutely not the case for the micro-hardness.

The opposite evolutions of wear resistance and micro-hardness appears to contradict classical abrasion test results. This nevertheless seems consistent with more realistic and complex loading conditions like drilling tests [16]. In fact fretting stressing not only includes abrasion but also oxidation and alternate cyclic loading. Hence in addition to micro-hardness other aspects like toughness and oxidation properties need to be considered. Finally it must be admitted that each test conclusion must be related and restricted to the corresponding studied stressing conditions. The challenge is then to simulate representative conditions by developing a simple and well instrumented laboratory test to build reliable wear models.

5. CONCLUSION.

Specific TiC-VC multilayer hard coatings obtained through an original and economical two step process which consists first in depositing PVD metallic multilayers on a HSS substrate and secondly applying a classical heat treatment (i.e. the carbide is generated by carbon diffusion from the substrate) have been studied. In an attempt to relate structural, morphological, hardness and tribological properties of TiC-VC multilayers, the following aspects have been highlighted :

- Xray patterns confirm that even for very thin modulation thicknesses, well-defined TiC and VC carbides are obtained. GDMS profiles conclude that, due to sublayer interdiffusion phenomena, the alternate TiC-VC tends to a pure mixed carbide structure when the modulation thickness falls below 100 nm.
- The microhardness variation as a function of the modulation thickness confirms a parabolic evolution with maximum hardness for a critical thickness around 50 nm. No direct correlation could be established between the multilayered structure and the microhardness. This hardness evolution is in fact consistent with Anderson and co-author models. It is linked to the dislocation moving force and the carbide micro and subsequent nano dimensions.
- Wear and friction properties have been characterised under gross slip fretting conditions. Taking into account the inter-diffusion mixed carbide structure, a “composite” approach has been developed. Unlike classical rules of mixtures, the modulation dependence of wear and friction is here considered. From the characterisation of the sublayers and the mixed carbide structure, reliable wear rate as a function the modulation thickness can be predicted. The friction evolution is less easily predicted due to the smoothing effect of the third body, which is currently not taken into account by the model.

Finally, it was shown that if micro-hardness evolution depends on the dislocation driving force and assumed to be carbide grain dimension dependent, the tribological properties, conversely, appear to be mainly controlled by the appearance and relative extension of the mixed carbide structure through the modulation element. The opposite evolution between wear resistance and micro-hardness has been observed, outlining the necessity of avoiding any direct prediction of a given tribological response from a plain micro-hardness measurement.

References:

- [1] K. Holmberg, H. Ronkainen, A. Matthews, *Ceramics International* 26 (2000), 787.
- [2] S.J. Bull, P.R. Chalkner, C. Johnston, V. Moore, *Surface & Coating Technology*, 68-69,(1994), 603.
- [3] H.J. Holleck, *Vac Sci Technology A*, 4, (1986), 261.
- [4] W. Schintlmeister, W. Wallgram, J. Kanz, K. Gigl, *Wear*, 100, (1984), 153.
- [5] Wendler, K. Jakubowski, Z. Has, Patent PL (Poland) No 167632 B1 (1995).
- [6] B. Wendler, *Surface & Coating Technology*, (1998), 276.
- [7] P. C. Yashar, W. D. Sproul, *Vacuum* 55, (1999), 179.
- [8] U. Helmersson, S. Todorova, S.A. Barnett, J.E. Sundgren, L.C. Market, J.E. Greene, J. *Appl. Phys.* , N° 62(2), (1987), 481.
- [9] X. Chu, S.A. Barnett, *J. Appl. Phys.*, N°77(9), (1995), 403.
- [10] P.M. Anderson, C. Li, *Nanostruct Mater*, N°5 (3), (1995), 349.
- [11] S. Fouvry, Ph. Kapsa, L.Vincent, *Wear* 200, (1996), 130.
- [12] J.F. Archard , *J. Appl. Phys.*, 24, (1953), 981
- [13] M. Berger, U. Wiklund, M. Eriksson, H. Engqvist, S. Jacobson, *Surf. And Coating Technology*, 116-119, (1999), 1138.
- [14] N. Axen, S. Jacobson, S. Hogmark, *Wear*, 203-204, (1997), 637.
- [15] H.C. Meng, K.C. Ludema, *Wear*, 181 - 183, (1995), 443.
- [16] V. Imbeni, C. Martini, E. Lanzoni, G. Poli, I.M. Hutchings, *Wear* 251, (2001), 997.